

# Onset of mid-crustal extensional flow in southern Tibet: Evidence from U/Pb zircon ages

Jeffrey Lee Department of Geological Sciences, Central Washington University, Ellensburg, Washington 98926, USA  
 Martin J. Whitehouse Laboratory for Isotope Geology, Swedish Museum of Natural History, Box 50007, SE-104 05 Stockholm, Sweden

## ABSTRACT

New ion microprobe U/Pb dates from zircon in deformed orthogneiss and migmatite and an undeformed granite in Mabja Dome are the first to constrain the timing of peak metamorphism, and onset and duration of mid-crustal ductile extension, in southern Tibet at  $35.0 \pm 0.8$  Ma and ~12–19 million years. The structural, metamorphic, and intrusive histories in mid-crustal rocks exposed in these north Himalayan gneiss domes are similar to those recorded in the Greater Himalayan sequence, suggesting that middle crust was continuous from beneath southern Tibet southward to the high Himalaya. Strain compatibility indicates that 35 Ma ductile extension in mid-crustal rocks of southern Tibet was accommodated to the south at shallow crustal levels via normal slip along the southern Tibetan detachment system, the oldest age estimate for slip along this normal fault zone, and extrusion of its footwall. If gravitational collapse is an additional important process driving extension, then southernmost Tibet may have been at or near maximum elevation by late Eocene–early Oligocene time.

**Keywords:** Tibet, U/Pb dating, zircon, north Himalayan gneiss domes, age dating, extensional tectonics, ductile flow.

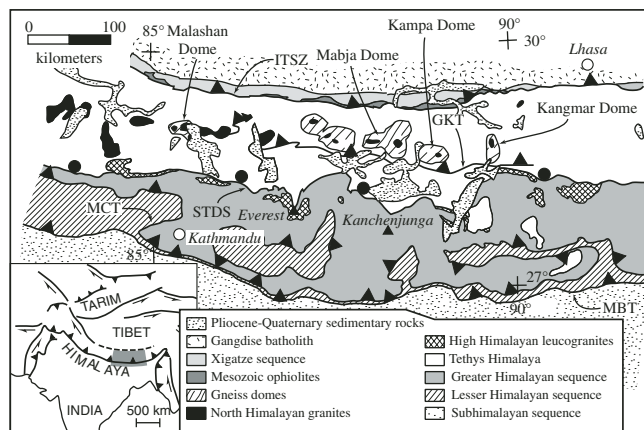
## INTRODUCTION

The Himalayan orogeny records Eocene to Holocene continental collision and convergence between India and Asia, and profound crustal thickening. However, extension parallel to convergence along the southern Tibetan detachment system (STDS) (e.g., Burg and Chen, 1984; Burchfiel et al., 1992) (Fig. 1) is an important structural element among the structural, thermal, and erosional processes that contribute to the development of the Himalayan orogenic belt. Gravitational collapse of overthickened, isostatically compensated continental crust was proposed earlier as a mechanism for development of the STDS (e.g., Burchfiel and Royden, 1985). More recently, southward extrusion of the Greater Himalayan sequence, i.e., high-grade metamorphic rocks and intrusions exposed in the footwall of the STDS and hanging wall of the Main Central thrust (MCT) (Fig. 1), driven by a low-

viscosity mid-crustal channel, a pressure gradient between Tibet and India, and surface denudation along the southern flank of the high Himalaya, has been postulated as the driving mechanism for the origin and evolution of the STDS (e.g., Beaumont et al., 2001; Hodges et al., 2001).

Geochronologic investigations of high-grade metamorphic and intrusive rocks in the Greater Himalayan sequence beneath and along the STDS indicate that ductile extension and brittle normal slip were ongoing during the early to middle Miocene (e.g., Murphy and Harrison, 1999; Searle et al., 2003, and references therein). These geochronologic data imply that maximum gravitational potential energy was reached and/or channel flow in the middle crust was ongoing by early Miocene time. However, the age of onset of ductile extension is unknown, yet crucial for characterizing the geodynamic evolution of the Himalayan orogeny.

**Figure 1. Regional tectonic map of central Himalaya orogen showing location of Mabja, Kangmar, Kampa, and Malashan domes. GKT—Gyirong-Kangmar thrust fault system; ITSZ—Indus-Tsangpo suture zone; MBT—Main Boundary thrust; MCT—Main Central thrust; STDS—Southern Tibetan detachment system. Thrust fault, teeth on hanging wall; normal fault, solid circle on hanging wall.**



The north Himalayan gneiss domes, southern Tibet, expose high-grade mid-crustal rocks that have undergone ductile extension linked to normal slip along the STDS (e.g., Chen et al., 1990; Lee et al., 2000, 2006; Aoya et al., 2005). In this paper we report the first ion microprobe U/Pb zircon ages from mid-crustal rocks of Mabja Dome (Fig. 1), the results of which constrain the onset of peak metamorphism and duration of ductile extension. These results have important implications for the geodynamics of southern Tibet.

## GEOLOGIC SETTING

Mabja is a 25-km-diameter doubly plunging antiformal core by migmatitic K-feldspar augen biotite orthogneiss and mantled by high-grade metapelite, granitic orthogneiss, and sediment at the highest structural levels (Lee et al., 2004) (Fig. 2). The orthogneiss and metasedimentary rock sequence were intruded by amphibolite dikes, a leucocratic dike swarm, and two-mica granites. Core and mantle rocks record two primary penetrative deformational

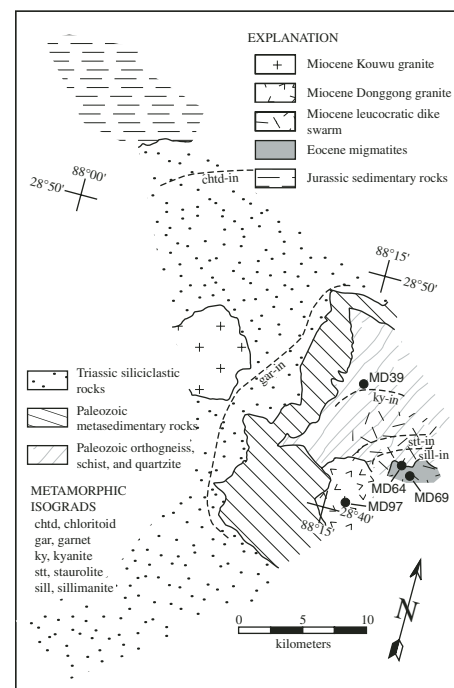


**Figure 2. Simplified geologic map of Mabja Dome showing metamorphic isograds (from Lee et al., 2004) and zircon U/Pb sample locations.**

events: an older contractional event, D1, characterized by ~E-W-trending folds of S0 with an associated N-dipping axial planar foliation, S1; and a younger vertical thinning and horizontal stretching event, D2, characterized by a mylonitic foliation, S2, associated N-S-trending mineral stretching lineation, and units vertically thinned by 50%–10%. Peak metamorphism ranged from ~475–530 °C and ~150–450 MPa in chloritoid-zone rocks to 705 ± 65 °C and 820 ± 100 MPa in sillimanite-zone rocks (Lee et al., 2004) (Fig. 2). Mesos-structural and microstructural textures indicate that peak metamorphism and generation of migmatites occurred post-D1 and syn-D2 ductile extension; emplacement of the leucocratic dike swarm was syn-D2 to late D2 deformation; and emplacement of two-mica granites was post-D2 deformation (Lee et al., 2004). Zircon U/Pb geochronology on the leucocratic dike swarm and one of the two undeformed two-mica granites yielded emplacement ages of 23.1 ± 0.8 Ma and 14.0–14.5 Ma, respectively (Lee et al., 2006; Zhang et al. 2004), indicating that D2 extension was ongoing at 23.1 Ma and had ceased by ca. 14.3 Ma.

#### U/PB ZIRCON AGE RESULTS

To determine the age of onset of peak metamorphism and duration of the high-strain D2 event, we completed U/Pb analyses of zircons from an orthogneiss, two migmatites, and a two-mica granite using a Cameca IMS1270 high mass resolution, high-sensitivity instrument. Sample localities, representative cathodoluminescence (CL) images, and age interpretative plots are shown in Figures 2, 3, and 4, respectively; analytical techniques, results of U-Th-Pb isotopic analyses, and age interpretative plots are given in the GSA Data Repository<sup>1</sup>.

#### Orthogneiss

CL images of zircons from sample MD39, a D2-deformed biotite + plagioclase + quartz + epidote granodiorite orthogneiss located just above the kyanite-in isograd (Fig. 2), show bright, low-U (140 ppm on average), oscillatory zoned cores grading into dark, high-U (5400 ppm on average), concordant homogeneous composition rims (Fig. 3A). Five core analyses yield a concordia age (sensu Ludwig, 1998) of 530 ± 9 Ma and four high-U rims plot discordantly; three of them are reverse discordant (Fig. 4A). Reverse discordance in high-U zircon may be attributed to problems with the U-Pb calibration that result from high levels of accumulated

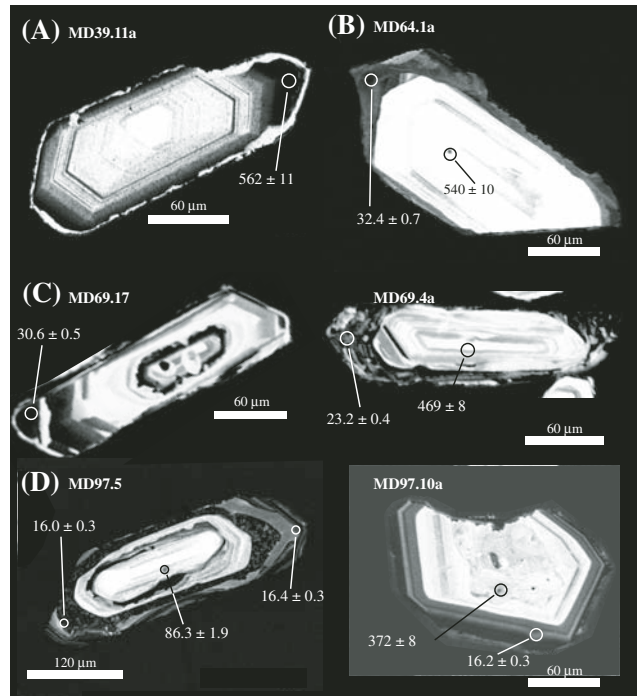


**Figure 3. Representative cathodoluminescence images (CL) of zircons from (A) orthogneiss sample MD39, (B) migmatite sample MD64, (C) migmatite sample MD69, and (D) two-mica granite sample MD97. Images show analyzed spots and corresponding 207-corrected ages (±1σ).**

radiation damage (e.g., McLaren et al., 1994), a process that does not affect the <sup>207</sup>Pb/<sup>206</sup>Pb ages. Normal discordance may reflect Pb loss, in this case probably during Miocene event(s), that will lead to a subhorizontal displacement from concordia, little affecting the <sup>207</sup>Pb/<sup>206</sup>Pb age. These four rim analyses yield a weighted average <sup>207</sup>Pb/<sup>206</sup>Pb age of 503 ± 18 Ma.

#### Migmatite

Zircons were analyzed from two D2-deformed migmatite samples: MD64, a sillimanite-bearing biotite + plagioclase + quartz + muscovite K-feldspar augen orthogneiss with local partial melt pockets, and MD69, a banded sillimanite-bearing biotite + plagioclase + quartz orthogneiss (Fig. 2). CL images show that MD64 zircons are characterized by bright, low-U (450 ppm on average) oscillatory zoned cores cut by concentric to convolutedly zoned recrystallized or newly grown, high-U (1760 ppm on average) rims (Fig. 3B). One core analysis yields a 207-corrected age of 734 ± 28 Ma and three additional cores may be used to define a concordia age of 527 ± 23 Ma (see footnote 1). The remaining 20 analyses represent zircon rims with high U contents (range 900–4800 ppm), low Th/U ratios (all <0.06, most <0.01), and a spread in age between ca. 500 Ma and 25 Ma. The 207-corrected ages for a prominent group of seven rims yield a weighted average of 35.0 ± 0.8 Ma (Fig. 4B). We interpret rims that are younger than this to represent Pb loss. Older rims are more difficult to interpret due to discordance (Pb loss), but the oldest near-concordant analyses point to a potential episode of rim growth at

491 ± 15 Ma, the weighted average <sup>207</sup>Pb/<sup>206</sup>Pb age from two grains. In CL images, zircons from sample MD69 exhibit bright, low-U (650 ppm on average) oscillatory zoned cores cut by dark, high-U (7080 ppm on average) homogeneous to spongy recrystallized or newly grown rims (Fig. 3C). Six core analyses yield a concordia age of 470 ± 8 Ma (see footnote 1). The 19 rim analyses yielded 3 distinct populations: (1) a single high-U (~10000 ppm) rim yields a <sup>207</sup>Pb/<sup>206</sup>Pb age of 484 ± 8 Ma, overlapping within error with the concordia age from the low-U cores, suggesting that this event may be related to a metamorphic episode somewhat younger than core ages for samples MD39 and MD64; (2) two low-Th (average Th/U ratio = 0.004) homogeneous to convolute rims (Fig. 3C) yield just overlapping 207-corrected ages of ca. 32 Ma (a third low-Th rim appears to yield a meaningless mixed age); and (3) 14 higher Th (average Th/U ratio = 0.12) spots are on spongy rims that have 207-corrected ages between 24.9 ± 0.8 Ma and 19.5 ± 0.8 Ma (Fig. 4C). Selected omission of grains from this latter group yields a statistically significant (i.e., low mean square of weighted deviates) weighted average. One rejection criterion assumes that the oldest ages are variably affected by overlap onto older high-U regions similar to that documented in the first population just described, and in this case, a subgroup of nine 207-corrected ages yielded a weighted average of 21.5 ± 0.4 Ma (Fig. 4C). An alternative rejection criterion assumes that the youngest ages have had some Pb loss; this subgroup of six 207-corrected ages yields a weighted average of 22.5 ± 0.6 Ma (Fig. 4C).

<sup>1</sup>GSA Data Repository item 2007018, analytical techniques, results of U-Th-Pb isotopic analyses, and age interpretative plots, is available online at [www.geosociety.org/pubs/ft2007.htm](http://www.geosociety.org/pubs/ft2007.htm), or on request from [editing@geosociety.org](mailto:editing@geosociety.org) or Documents Secretary, GSA, P.O. Box 9140, Boulder, CO 80301, USA.

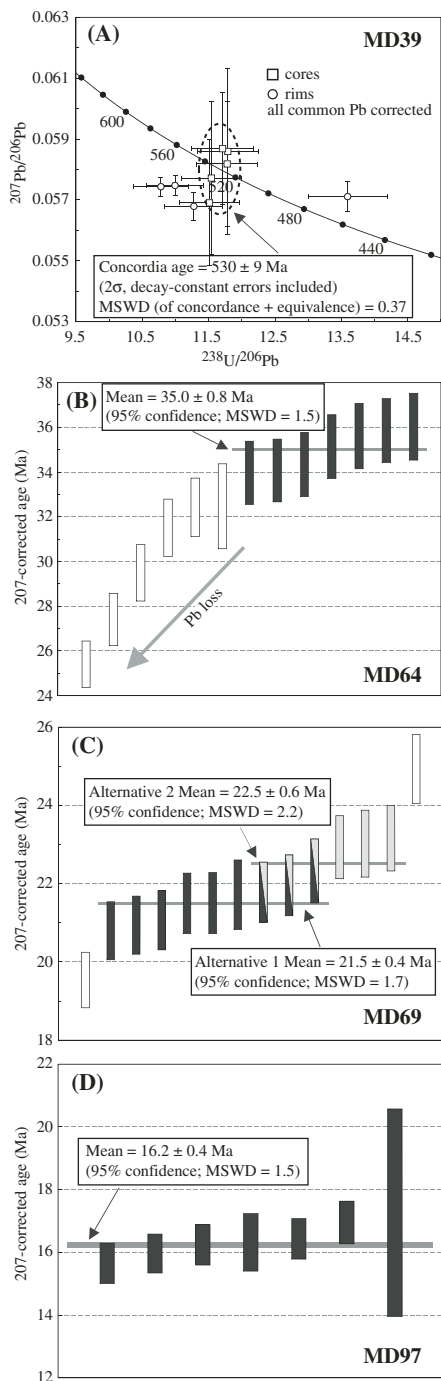


**Figure 4.** Interpretative plots of zircon data (all error symbols shown at  $2\sigma$  level). **A:** Inverse concordia plot of data from orthogneiss sample MD39. **B:** Weighted average of  $^{207}\text{Pb}$ -corrected ages from migmatite sample MD64 (filled error bars are included in indicated mean; open error bars, interpreted as Pb loss, are omitted). **C:** Weighted average of  $^{207}\text{Pb}$ -corrected ages from migmatite sample MD69 showing two alternative results (open error bars are omitted from both means; black and gray-black points are included in alternative 1; gray and gray-black points are included in alternative 2). **D:** Weighted average of  $^{207}\text{Pb}$ -corrected ages from two-mica granite sample MD97. MSWD—mean square of weighted deviates.

## Two-Mica Granite

In CL, zircons from the postdeformation, two-mica Donggong granite (sample MD97, Fig. 2) show bright, relatively low U (1100 ppm on average), oscillatory zoned to homogeneous cores cut by darker, high-U (6110 ppm on average) recrystallized or newly grown oscillatory rims (Fig. 3D). Of five core analyses, one indicates a minimum  $^{207}\text{Pb}/^{206}\text{Pb}$  age of  $\sim 1640$  Ma, two yield a weighted average  $^{207}\text{Pb}/^{206}\text{Pb}$  age of  $518 \pm 36$  Ma, and two others are likely younger than this but highly discordant. A weighted average of the  $^{207}\text{Pb}$ -corrected ages from all seven rim analyses yields an age of  $16.2 \pm 0.4$  Ma (Fig. 4D).

## INTERPRETATION

Oscillatory zoning and high Th/U ratios ( $>0.1$ – $0.2$ ) in MD39, MD64, MD69, and MD97 zircon cores indicate that these are igneous in origin and xenocrystic (e.g., Vavra et al., 1999; Rubatto and Gebauer, 2000). MD39, MD64, and MD97 yield equivalent core ages of 530–518 Ma, similar to the 566–507 Ma age for the Kangmar granite (Scharer et al., 1986; Lee et al., 2000) (Fig. 1), demonstrating that these granite orthogneisses were part of an early Paleozoic magmatic event preserved in pre-Himalayan crust (cf. Miller et al., 2001). Cores from MD69 zircons yield a somewhat younger early Paleozoic age of ca. 470 Ma, implying two early Paleozoic magmatic events.

Zircons from deformed orthogneiss MD39, which underwent Barrovian metamorphic temperatures of between  $575 \pm 50$  °C and  $620 \pm 51$  °C (Lee et al., 2004), do not exhibit newly grown or recrystallized rims, suggesting that metamorphic temperatures were not sufficiently high for such growth. This interpretation is consistent with observations that zircon does not react to metamorphism at temperatures below  $\sim 700$  °C and in the absence of anatexis (Vavra et al., 1999; Rubatto et al., 2001). The two deformed migmatites underwent Barrovian metamorphic temperatures of  $>705 \pm 65$  °C, began to partially melt to form migmatites (Lee et al., 2004), and exhibit low Th/U ratio (0.004) zircon rims, commonly assigned to metamorphic zircon (e.g., Vavra et al., 1999; Rubatto and Gebauer, 2000), demonstrating that these rocks were at conditions appropriate for new zircon growth or recrystallization during metamorphism. We interpret the rim ages of 35–32 Ma from these samples as the time of new zircon growth or recrystallization during Barrovian metamorphism. Peak metamorphic conditions at these depths were either prolonged, initiating at 35 Ma and continuing to at least 32 Ma, or hydrothermal activity reset MD69 zircon rims to 32 Ma. Because metamorphism and migmatization were synchronous with D2 ductile extension (Lee et al., 2004), the 35 Ma age also defines the onset of this mid-crustal deformation event.

Spongy texture is characteristic of the ca. 22 Ma zircon rims from migmatite sample MD69; such zircon textures have been interpreted as forming during hydrothermal fluid migration (e.g., Hoskin et al., 1998). If this interpretation is correct, then hydrothermal migration may have initiated following emplacement of the late-D2 deformation leucocratic dike swarm at  $23.1 \pm 0.8$  Ma (Lee et al., 2006).

The young zircon rims from the undeformed granite MD97 exhibit oscillatory zoning, suggesting new igneous growth at 16.2 Ma on older xenocrystic cores after D2 deformation had ceased.

## DISCUSSION AND CONCLUSIONS

Our new U/Pb zircon ion probe ages, combined with structural, quantitative metamorphic petrology, and U/Pb zircon age data from Mabja (Lee et al., 2004; 2006), indicate that high-strain D2 extension, synchronous with peak metamorphism and generation of migmatites, initiated at  $35.0 \pm 0.8$  Ma, was ongoing at  $23.1 \pm 0.8$  Ma, and had ceased by  $16.2 \pm 0.4$  Ma. Our results suggest that D2 deformation was prolonged, lasting  $\sim 12$ – $19$  m.y.

To the south of the north Himalayan gneiss domes, the Greater Himalayan sequence (Fig. 1) is characterized by middle crust composed of strongly deformed late Eocene to early Oligocene Barrovian-grade metasedimentary, orthogneissic, and migmatitic rocks, and early Oligocene to middle Miocene deformed and undeformed leucogranites (e.g., Murphy and Harrison 1999; Vance and Harris 1999; Walker et al., 1999; Simpson et al., 2000; Searle et al., 2003). The structural, metamorphic, anatectic, and intrusive histories in these rocks are similar to those recorded in the north Himalayan gneiss domes. These similarities suggest that from late Eocene–early Oligocene to middle Miocene time, high-grade mid-crustal metasedimentary and orthogneissic rocks, crosscut by anatectic melts and leucogranites, were continuous from beneath southern Tibet southward to the high Himalaya.

Lee et al. (2000, 2006) argued that, to maintain strain compatibility, D2 ductile flow in the North Himalayan gneiss domes was accommodated at shallow crustal levels to the south by normal sense (top to north) slip along the STDS. Given our new U/Pb age data, and those of Lee et al. (2006), this interpretation implies that normal ductile shearing in the footwall of the STDS and brittle slip along the STDS began at 35 Ma, was ongoing at 23 Ma, and ceased by 16 Ma. Although the 23–16 Ma history of ductile extension in the middle crust of southern Tibet is compatible with estimates for the minimum age of normal shear and brittle slip along the STDS (Murphy and Harrison 1999; Searle et al. 2003, and references therein), an out-

come of this interpretation is that initiation of slip along the STDS is significantly older than generally thought. Moreover, no net extension across the STDS (e.g., Searle et al., 2003) and strain compatibility dictate that mid-crustal D2 ductile flow in southern Tibet must have been accommodated by its southward extrusion (e.g., Nelson et al. 1996; Hodges et al., 2001) since late Eocene–early Oligocene time. Exposures of the Greater Himalayan sequence have been interpreted as the leading edge of this southward-extruding and eroding channel of ductile mid-crustal rocks bounded above by the STDS and below by the MCT (e.g., Grujic et al., 1996; Beaumont et al., 2001). Our ca. 35 Ma age for the onset of mid-crustal extension and strain compatibility implies that slip along both the MCT and STDS must have initiated at that time.

Our data do not preclude gravitational collapse as an additional contributing mechanism driving mid-crustal extension in southern Tibet. If gravitational collapse is an important process, a potential outcome of our geochronologic data is that by late Eocene–early Oligocene time, the crust was thickened sufficiently such that southernmost Tibet was at or near maximum elevation. Stable isotopic data from sedimentary basins suggest that the southern and central Tibetan Plateau has remained at constant high elevation (~4–5 km) for at least the past 35 m.y. (Rowley and Currie, 2006), supporting this interpretation. Regardless, our conclusions imply that a dynamic steady state between crustal thickening, which increased gravitational potential energy, and southward extrusion and/or gravitational collapse, which decreased that potential energy, persisted for at least ~20 m.y. in southernmost Tibet.

#### ACKNOWLEDGMENTS

Discussions with B. Hacker, P. Hoskin, and S. Wallis were helpful. Funding was provided by Central Washington University and National Science Foundation grant EAR-9526861. The Nordsim facility is operated under an agreement between the research councils of Denmark, Norway, and Sweden, the Geological Survey of Finland, and the Swedish Museum of Natural History. Nordsim contribution 155.

#### CITED

Aoya, M., Wallis, S.R., Terada, K., Lee, J., Kawakami, T., Wang, Y., and Heizler, M., 2005, North-south extension in the Tibetan crust triggered by granite emplacement: *Geology*, v. 33, p. 853–856, doi: 10.1130/G21806.1.

Beaumont, C., Jamieson, R.A., Nguyen, M.H., and Lee, B., 2001, Himalayan tectonics explained by extrusion of a low-viscosity crustal channel coupled to focused surface denudation: *Nature*, v. 414, p. 738–742, doi: 10.1038/414738a.

Burchfiel, B.C., and Royden, L.H., 1985, North-south extension within the convergent Himalayan

region: *Geology*, v. 13, p. 679–682, doi: 10.1130/0091-7613(1985)13<679:NEWTCH>2.0.CO;2.

Burchfiel, B.C., Zhiliang, C., Hodges, K.V., Yuping, L., Royden, L.H., Changrong, D., and Jiene, X., 1992, The south Tibetan detachment system, Himalayan orogen: Extension contemporaneous with and parallel to shortening in a collisional mountain belt: *Geological Society America Special Paper* 269, 41 p.

Burg, J.P., and Chen, J.M., 1984, Tectonics and structural zonation of southern Tibet, China: *Nature*, v. 311, p. 219–223, doi: 10.1038/311219a0.

Chen, Z., Liu, Y., Hodges, K.V., Burchfiel, B.C., Royden, L.H., and Deng, C., 1990, The Kangmar Dome: A metamorphic core complex in southern Xizang (Tibet): *Science*, v. 250, p. 1552–1556.

Grujic, D., Casey, M., Davidson, C., Hollister, L.S., Kundig, R., Pavlis, T., and Schmid, S., 1996, Ductile extrusion of the High Himalayan Crystalline in Bhutan: Evidence from quartz microfabrics: *Tectonophysics*, v. 260, p. 21–43, doi: 10.1016/0040-1951(96)00074-1.

Hodges, K.V., Hurtado, J.M., and Whipple, K.X., 2001, Southward extrusion of Tibetan crust and its effect on Himalayan tectonics: *Tectonics*, v. 20, p. 799–809, doi: 10.1029/2001TC001281.

Hoskin, P.W.O., Kinny, P.D., and Wyborn, D., 1998, Chemistry of hydrothermal zircon: Investigation timing and nature of water-rock interaction, in Arehart, G.B., and Hulston, J.R., eds., *Water-Rock Interaction, WRI-9*: Rotterdam, The Netherlands, Balkema, p. 545–548.

Lee, J., Dinklage, W.S., Hacker, B.R., Wang, Y., Gans, P.B., Calvert, A., Wan, J., Chen, W., Blythe, A., and McClelland, W., 2000, Evolution of the Kangmar Dome, southern Tibet: Structural, petrologic, and thermochronologic constraints: *Tectonics*, v. 19, p. 872–896, doi: 10.1029/1999TC001147.

Lee, J., Hacker, B.R., and Wang, Y., 2004, Evolution of North Himalayan gneiss domes: Structural and metamorphic studies in Mabja Dome, southern Tibet: *Journal of Structural Geology*, v. 26, p. 2297–2316, doi: 10.1016/j.jsg.2004.02.013.

Lee, J., McClelland, W., Wang, Y., Blythe, A., and McWilliams, M., 2006, Oligocene-Miocene middle crustal flow in southern Tibet: Geochronologic studies in Mabja Dome, in Law, R.D., et al., eds., *Channel flow, ductile extrusion and exhumation in continental collision zones*: Geological Society [London] Special Publication 268, p. 445–469 (in press).

Ludwig, K.R., 1998, On the treatment of concordant uranium-lead ages: *Geochimica et Cosmochimica Acta*, v. 62, p. 665–676, doi: 10.1016/S0016-7037(98)00059-3.

McLaren, A.C., FitzGerald, J.D., and Williams, I.S., 1994, The microstructure of zircon and its influence on the age determination from Pb/U isotopic ratios measured by ion microprobe: *Geochimica et Cosmochimica Acta*, v. 58, p. 993–1005, doi: 10.1016/0016-7037(94)90521-5.

Miller, C., Thoni, M., Frank, W., Grasemann, B., Klotzli, U., Guntli, P., and Draganits, E., 2001, The early Palaeozoic magmatic event in the Northwest Himalaya, India: Source, tectonic setting and age of emplacement: *Geological Magazine*, v. 138, p. 237–251, doi: 10.1017/S0016756801005283.

Murphy, M.A., and Harrison, T.M., 1999, Relationship between leucogranites and the Qomolangma detachment in the Rongbuk Valley, south Tibet: *Geology*, v. 27, p. 831–834, doi: 10.1130/0091-7613(1999)027<0831:RBLATQ>2.3.CO;2.

Nelson, K.D., and 27 others, 1996, Partially molten middle crust beneath southern Tibet: Synthesis of project INDEPTH results: *Science*, v. 274, p. 1684–1688, doi: 10.1126/science.274.5293.1684.

Rowley, D.B., and Currie, B.S., 2006, Palaeo-altimetry of the late Eocene to Miocene Lunpola basin, central Tibet: *Nature*, v. 439, p. 677–681, doi: 10.1038/nature04506.

Rubatto, D., and Gebauer, D., 2000, Use of cathodoluminescence for U-Pb zircon dating by ion microprobe: Some examples from the western Alps, in Pagel, M., et al., eds., *Cathodoluminescence in geosciences*: Berlin, Springer, p. 373–400.

Rubatto, D., Williams, I.S., and Buick, I.S., 2001, Zircon and monazite response to prograde metamorphism in the Reynolds Range, central Australia: Contributions to Mineralogy and Petrology, v. 140, p. 458–468, doi: 10.1007/PL00007673.

Scharer, U., Xu, R., and Allegre, C., 1986, U-(Th)-Pb systematics and ages of Himalayan leucogranites, south Tibet: *Earth and Planetary Science Letters*, v. 77, p. 35–48, doi: 10.1016/0012-821X(86)90130-5.

Searle, M.P., Simpson, R.L., Law, R.D., Parrish, R.R., and Waters, D.J., 2003, The structural geometry, metamorphic and magmatic evolution of the Everest massif, High Himalaya of Nepal-South Tibet: *Geological Society [London] Journal*, v. 160, p. 345–366.

Simpson, R.L., Parrish, R.R., Searle, M.P., and Waters, D.J., 2000, Two episodes of monazite crystallization during metamorphism and crustal melting in the Everest region of the Nepalese Himalaya: *Geology*, v. 28, p. 403–406, doi: 10.1130/0091-7613(2000)028<0403:TEOMCD>2.3.CO;2.

Vance, D., and Harris, N., 1999, The timing of prograde metamorphism in the Zaskar Himalaya: *Geology*, v. 27, p. 395–398, doi: 10.1130/0091-7613(1999)027<0395:TOPMIT>2.3.CO;2.

Vavra, G., Schmid, R., and Gebauer, D., 1999, Internal morphology, habit and U-Th-Pb microanalysis of amphibolite-to-granulite facies zircons: Geochronology of the Ivrea Zone (Southern Alps): Contributions to Mineralogy and Petrology, v. 134, p. 380–404, doi: 10.1007/s004100050492.

Walker, J.D., Martin, M.W., Bowring, S.A., Searle, M.P., Waters, D.J., and Hodges, K.V., 1999, Metamorphism, melting, and extension: Age constraints from the High Himalayan slab, S.E. Zaskar and N.W. Lahoul: *Journal of Geology*, v. 107, p. 473–495, doi: 10.1086/314360.

Zhang, H., Harris, N., Parrish, R., Kelley, S., Zhang, L., Rogers, N., Argles, T., and King, J., 2004, Causes and consequences of protracted melting of the mid-crust exposed in the North Himalayan antiform: *Earth and Planetary Science Letters*, v. 228, p. 195–212, doi: 10.1016/j.epsl.2004.09.031.

Manuscript received 25 March 2006

Revised manuscript received 11 August 2006

Manuscript accepted 17 August 2006

Printed in USA